ISSN 0742-0463, Journal of Volcanology and Seismology, 2021, Vol. 15, No. 3, pp. 180–200. © Pleiades Publishing, Ltd., 2021.
Russian Text © The Author(s), 2021, published in Vulkanologiya i Seismologiya, 2021, No. 3, pp. 41–62.

The Tephra of the 1669 Etna, Sicily Eruption: The Petrologic, Mineralogical, Geochemical Properties, and the Geodynamic Aspect

V. I. Silaev[a], *, G. A. Karpov[b], **, L. P. Anikin[b], V. Scribano[c], D. N. Remizov[d], *, V. N. Filippov[a], D. V. Kiseleva[e], ****, B. A. Makeev[a], S. N. Shanina[a], K. V. Tarasov[b], and C. K. Simakov[f]**

[a] *Institute of Geology, Federal Research Center, Komi Science Center, Ural Branch, Russian Academy of Sciences, ul. Pervomaiskaya, 54, Syktyvkar, 167982 Russia*

[b] *Institute of Volcanology and Seismology, Far East Branch, Russian Academy of Sciences, bulvar Piipa, 9, Petropavlovsk-Kamchatsky, 683006 Russia*

[c] *University of Catania, Department of Biological, Geological and Environmental Sciences, Universitetskaya pl., 2, Catania, 57, 95129 Italy*

[d] *All-Russia Rosnedra Geological Institute, Sredny pr., 74, VO, St. Petersburg, 199106 Russia*

[e] *Institute of Geology and Geochemistry, Ural Branch, Russian Academy of Sciences, ul. Vonsovskogo, 15, Yekaterinburg, 20016 Russia*

[f] *ADAMANT, Skolkovo Innovation Center, Tikhoretsky pr., 10/1-61, St. Petersburg, 194064 Russia*

**e-mail: silaev@geo.komisc.ru*

***e-mail: karpovga@ksnet.ru*

****e-mail: dnr1957@yandex.ru*

*****e-mail: podarenka@mail.ru*

Received July 15, 2020; revised August 10, 2020; accepted December 11, 2020

Abstract—This paper reports the first multidisciplinary petrologic, mineralogical, and geochemical studies of the near-crater tephra discharged by the 1669 catastrophic eruption of Etna stratovolcano, Sicily. We studied the grain-size distribution, chemical and mineral-phase composition of the tephra. We determined the composition of trace elements and the composition of encapsulated lithogenic gases. Etna is classified as an intraplate volcano with a deep-seated magma chamber. Of special importance is the fact that the Etnean products were found to contain volcanogenic organoids that have phase, elemental, and isotope compositions similar to the organoids encountered in diamond-bearing products discharged by some Kamchatka volcanoes. This corroborates out earlier inference that carbonaceous abiogenesis is ubiquitous in the conditions of onshore volcanism.

Keywords: Etna, tephra, intraplate volcanoes, trace elements, lithogenic gases, organoids, carbonaceous abiogenesis under volcanic conditions

DOI: 10.1134/S0742046321020056

INTRODUCTION

The Etna stratovolcano is one of the most active volcanoes in the world. It is situated in the east of Sicily, southern Italy, in the middle of the Mediterranean Sea (Fig. 1). At present, the volcanic edifice occupies an area of about 1260 km^2, while its summit is at an absolute height of 3340 m. Etna has had a long history of geological evolution, showing a nearly continuous activity since at least the Middle Pleistocene (Svyatlovsky and Kitaigorodsky, 1988). As an example, major eruptions took place in 1911, 1928, 1949, 1950–1951, 1964, 1968, 1971, 1983, 1989, 1990, and 1991–1993, citing the greatest events for the 20th century. However, the volcanologists were struck, not only by the high activity of Etna, but also by the rate at which the volcanic edifice was modified in outward appearance (Tazieff, 1978; *Encyclopedia ...,* 1999).

The modern volcano stands on a thick, tectonized volcanogenic–sedimentary basement dating back to Miocene–Early Pleistocene time, being 1300 m above sea level in the western sector of the edifice. The E-NE side of the volcano descends to the shoreline to make the Valle del bove volcano-tectonic basin 8 by 4 km in size. Although the basin bottom is completely overlain by relatively recent lava flows, its inner slope still preserves a few relicts of older eruptions.

Mt. Etna is a coarse-layered, conical volcano with an open conduit and eruptions that occur through four summit vents in an unorderly manner. Etna's activity is seen, first, as degassing with insignificant discharges of ash lasting a few months to a few years, secondly, as

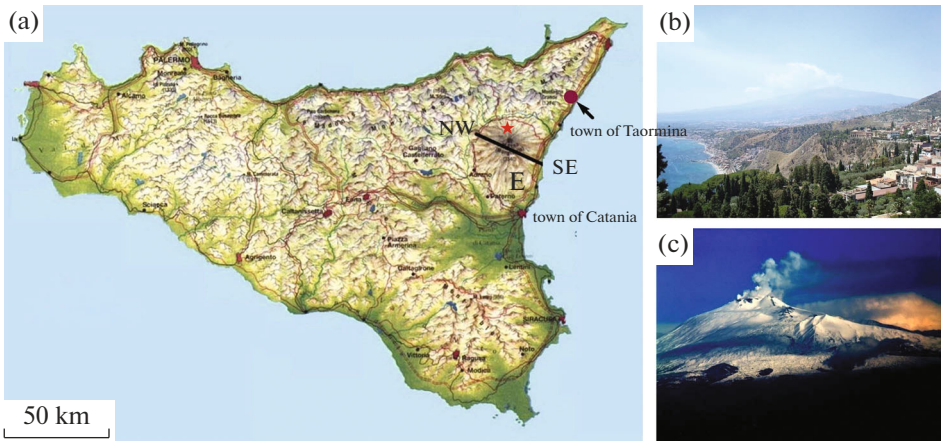

Fig. 1. Sicily (a): E stands for Mt. Etna, NW–SE marks the traverse for reconstructing the geological history of the volcano), view to Mt. Etna from a historical settlement, town of Taormina (b), and a recent Etna eruption (c). The red star marks the sampling site where material was taken for our study.

rhythmic eruptions of lava clots and pyroclastic bombs (the Strombolian type of eruption), and thirdly, as discrete powerful spurts and flows of lava (the Hawaiian type) or as violent explosions discharging great amounts of lava and ash (the Plinian type of eruption). In addition, there have been short-lived lava flows discharged from one or several central vents in combination with lava spurts. Parasitic fissure eruptions are rather frequent as well. All slopes of Mt. Etna at different heights are spotted with scoria cones and lava flows discharged during prehistorical and historical time.

According to geological data (Branca et al., 2011a, b; De Beni et al., 2011), the present-day Etna is a cluster of several edifices that were successively evolving during the long history of volcanic edifices (Romano, 1982). The recorded magmatic activity of Mt. Etna dates back to approximately 500 ka (the earlier half of the Middle Pleistocene), showing as subvolcanic emplacements in a Miocene to Early Pleistocene volcanogenic-sedimentary rock sequence (Fig. 2, traverse 1) both on land and in a wide bay that covered part of the modern Etna area during that time. The associated magma was tholeiitic and showed geochemical affinity to both normal (N-MORB) and enriched (E-MORB) MOR basalts (Fig. 3). Soon after that, a subaerial volcanic shield edifice appeared, to be partially destroyed during the period of temporary suspension of volcanic activity. The products of the next powerful volcanic rise of activity starting approximately 170 ka ago (the end of the Middle Pleistocene) and lasting until the present are dominated by trachybasalts (see Fig. 2, traverses 2–5), which have geochemical and isotope-geochemical features proper to basaltoids of oceanic islands, OIB.

The petrologic and geochemical features of the volcanics, as well as the character of Etnean eruptions, point to an extensional tectonic setting. That fact can serve as supporting the hypothesis that Etna is an extension, in space and time, of the Mesozoic–Cenozoic basaltic magmatic activity of the neighboring Hyble area in southeastern Sicily. The volcanic activity in the area was evolving in relation to fault tectonics, frequently along linear underwater fissures, more rarely as central volcanoes like the oceanic island type. On the contrary, the history of Etnean eruptions can hardly be thought related to geodynamic models that deal with volcanism at the boundaries of convergent plates, in particular, the African and Eurasian plates.

The geodynamic nature of Mt. Etna as a volcano, hence of the entire central Mediterranean region, still remains a debatable issue. To take an example, the analysis of seismic data suggested (Finetti, 1982) that the lithosphere beneath the Ionian basin, in eastern Sicily, is a relict of the Tethys Ocean dating back to Late Paleozoic and Early Mesozoic time. Vai (1994, 2003) studied the distribution of deep-sea Permian fauna in several Mediterranean regions to conclude that the basement beneath Sicily is a relict of the Ionian branch of the Tethys, which is also known as the Oman–Iraq–Levant–Sicily–Texas sea chain. Nevertheless, several authors seriously doubt the idea of an Ionian–Sicilian lithosphere continuity, because they think that eastern Sicily is a fragment of a passive continental margin, while treating Sicily and Etna as elements of the African continental plate (BenAvraham et al., 1990). The results of geophysical studies in the region do not lend themselves to a definitive geodynamic diagnosis, seeing that they fit both the hypothesis of a thin continental crust there (Chironi et al., 2000) and the hypothesis of a strongly serpentinized oceanic lithosphere (Giampiccolo et al., 2017).

The 30-year petrologic study of deep-seated xenoliths recovered from the diatremes in the Hyblean area (Scribano et al., 2006a, b; Manuella et al., 2015) provide convincing proof that the subsided basement

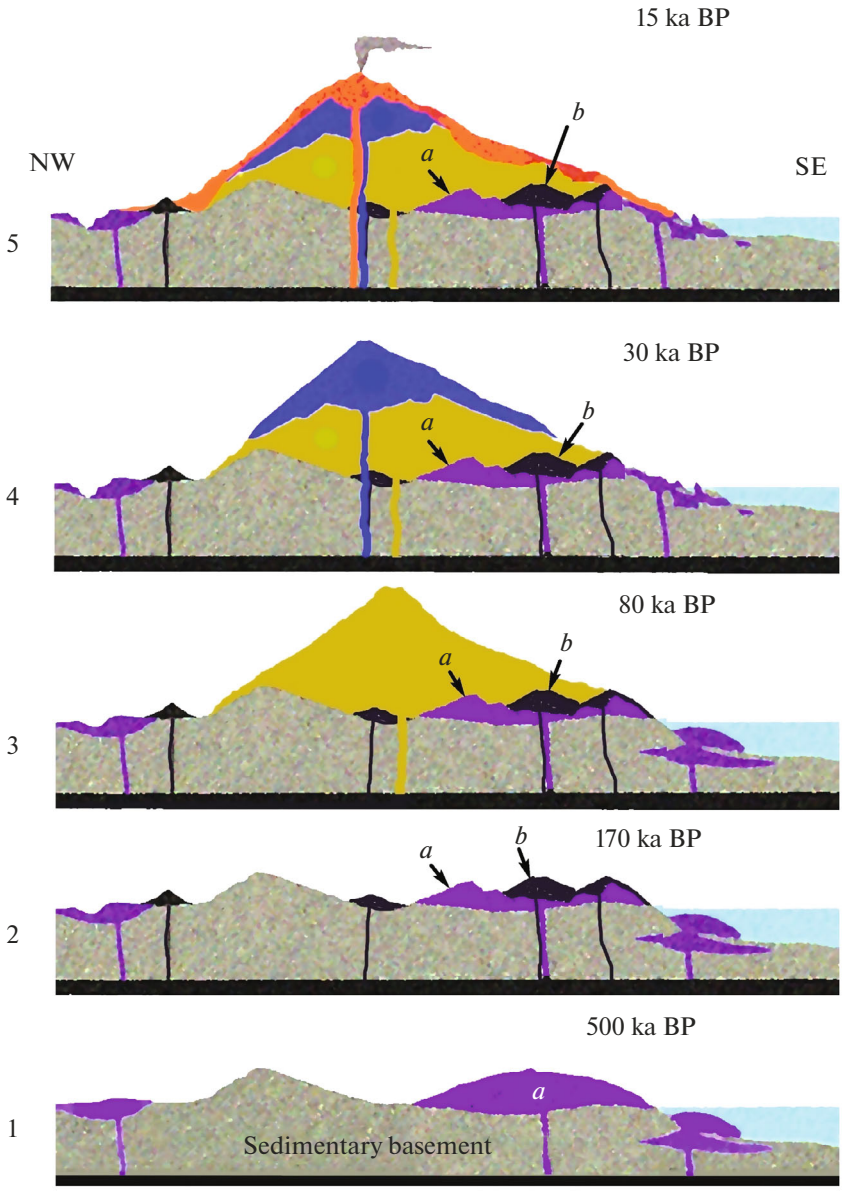

Fig. 2. The geological history of Mt. Etna as characterized by a chronological decomposition of the geological section along the NW–SE line (see Fig. 1). Phases: (1) discharge of early tholeiitic basalts (a); (2) the appearance of first alkaline basalts (b); (3–5) successive formation of volcanic edifices, namely, Trifoglietto, the earlier and later Mongibello, respectively. After Romano (1982) with some simplification.

beneath southeastern Sicily is of paleo-oceanic origin and is historically connected to the Tethus paleo-ocean. For this reason we should regard the Ionian edge of the area as part of the paleo-ocean, while the entire eastern margin of Sicily and its underwater southward extension along the pelagic shelf should be treated as a relict of the Tethys (Scribano et al., 2006a) or as part of an oceanic fault zone. Based on these considerations, Mt. Etna can be regarded as an OIB volcano sitting on a paleo-oceanic crust (see Fig. 3). The detection of serpentinites at depth beneath Mt. Etna can become the key factor showing that the Etnean eruptions involved deep-seated magmas enriched in magnesium (Correale et al., 2019).

Approximately 30 eruptions interrupted by repose periods of varying length have been recorded on Mt. Etna during the entire historical period from 1226 BC until the present. The interruptions varied in the range 1047–78 years until 1669 and 197–6 years between 1669 and 1971, while those between 1971 and the present time have become as short as 9–1 years. From this it follows that the frequency of Etnean eruptions obviously tends to increase by a factor of many times during the historical period; that is to say, the

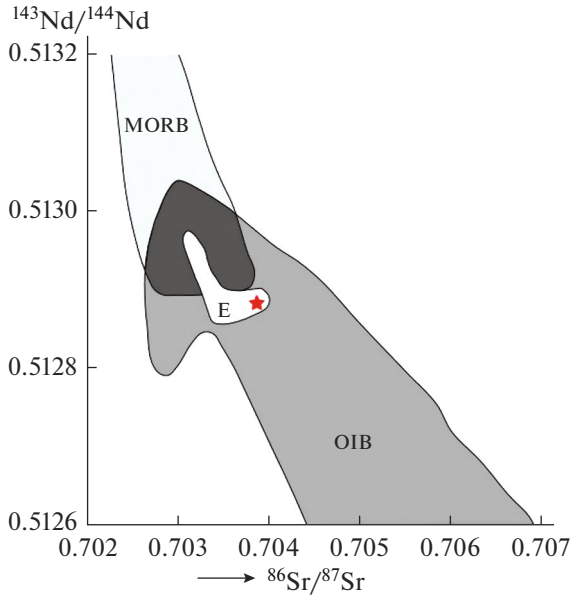

Fig. 3. The isotope diagnostics of the primary substratum in the products of the 1669 Etnean eruption (the *E* field where the star marks the data point for the isotope composition of the sample investigated). The reference fields: MORB MOR basalt and OIB oceanic island basalt (Tonarini et al., 1996).

frequency has sharply increased during the past 50 years. As well, the French and Italian volcanologists think that the character of Etnean eruptions has changed from dominantly effusive to dominantly explosive during recent years.

Roughly the same inference can be made from an analysis of the frequency of Etnean disastrous eruptions. These were four during the historical period of interest, viz., in 122, 1169, 1669, and 1928. The eruptions destroyed dozens of population centers and killed 50 to 150 thousand people. It can be seen from the above dates that the interval between the first and the second eruption was 1047 years, that between the second and the third was shorter, 500 years, while the interval between the third and fourth did not reach 260 years. That is to say, if we take the case of catastrophic eruptions, one also has an obvious acceleration of the associated frequency. Simple extrapolation shows that the next catastrophic eruption of Mt. Etna is to be expected around 2040.

Of those which have occurred, it is the 1669 eruption which seems the most disastrous (Corsaro et al., 1996). As the well-known volcanologist Tazieff said, it was "an appalling calamity, when it seems the very cyclopes sitting in the interior of the mount rose" (Tazieff, 1978). The eruption started with discharge of ash from a bocca (hole) at a height of 2200 m, subsequently the explosive phase was replaced with an effusive. The rate of basaltic lava discharged from the vent reached 5.7 m^3/s, its total volume being estimated as 231 × 10^6 m^3 (*Encyclopedia ...,* 1999); the eruption lasted 471 days. The number of casualties is estimated as 15–100 thousand people[1].

Because the eruption had a large amount of energy, an enormous mass of pyroclastic material was discharged onto the ground surface, in addition to lavas, and this material has been well preserved on lava flows until today. The study of the material is of considerable interest, considering that it is little known compared with the lava products. The task is especially urgent in connection with the prediction of an approaching catastrophic eruption.

THE OBJECT OF STUDY AND THE METHODS

The object of study was a large sample of deposited ash (tephra) of brown color which was taken by the Italian volcanologist Vittorio Scribano in 2018 at the southern base of the scoria cone produced by the 1669 catastrophic eruption of Mt. Etna (Fig. 4). The eruption started on March 11, 1669 from a fissure lying at an approximate height of 800 m above sea level on the south slope of Etna. The eruption first produced a large scoria cone that was called Monti Rossi afterwards. The next to come was lava, which was flowing round topographic highs, streaming down the south slope and devastating everything in its path. In late March the lava flow whose front was 2 km wide reached the Catania city walls and went down into the sea by April 23. Lava continued flowing underground through a system of lava pipes during the subsequent two months, so nobody knew the exact date the eruption ceased.

Our studies of the tephra used the following techniques: grain-size measurement, X-ray diffractometry (Shimadzu XRD-6000); Raman spectroscopy (LabRam HR800 Horiba, He-Ne 632.8-nm laser); analytical scanning electron microscopy (JSM-6400 with EDX and wave spectrometers); mass spectrometry with inductively coupled plasma (Perkin Elmer ELAN 9000; X-ray fluorescence spectrometry (Shimadzu XRF-1800, Analyst S.T. Neverov); isotope spectrometry (Delta V+ (Finnigan) with a Flash EA-HT 1112 element analyzer and a Confo IV gas switch; Analyst I.V. Smoleva); gas chromatography (Tsvet-800 with a pyrolysis device). ICP-MS trace element analysis was performed at the *Geoanalitik* TsKP UrO RAN. The other determinations were carried out at the *Geonauka TsKP*, Institute of Geology, Komi Federal Research Center, Science Center, Ural Branch, Russian Academy of Sciences (town of Syktyvkar).

[1] For comparison: the AD79 eruption of Vesuvius killed roughly two thousand people.

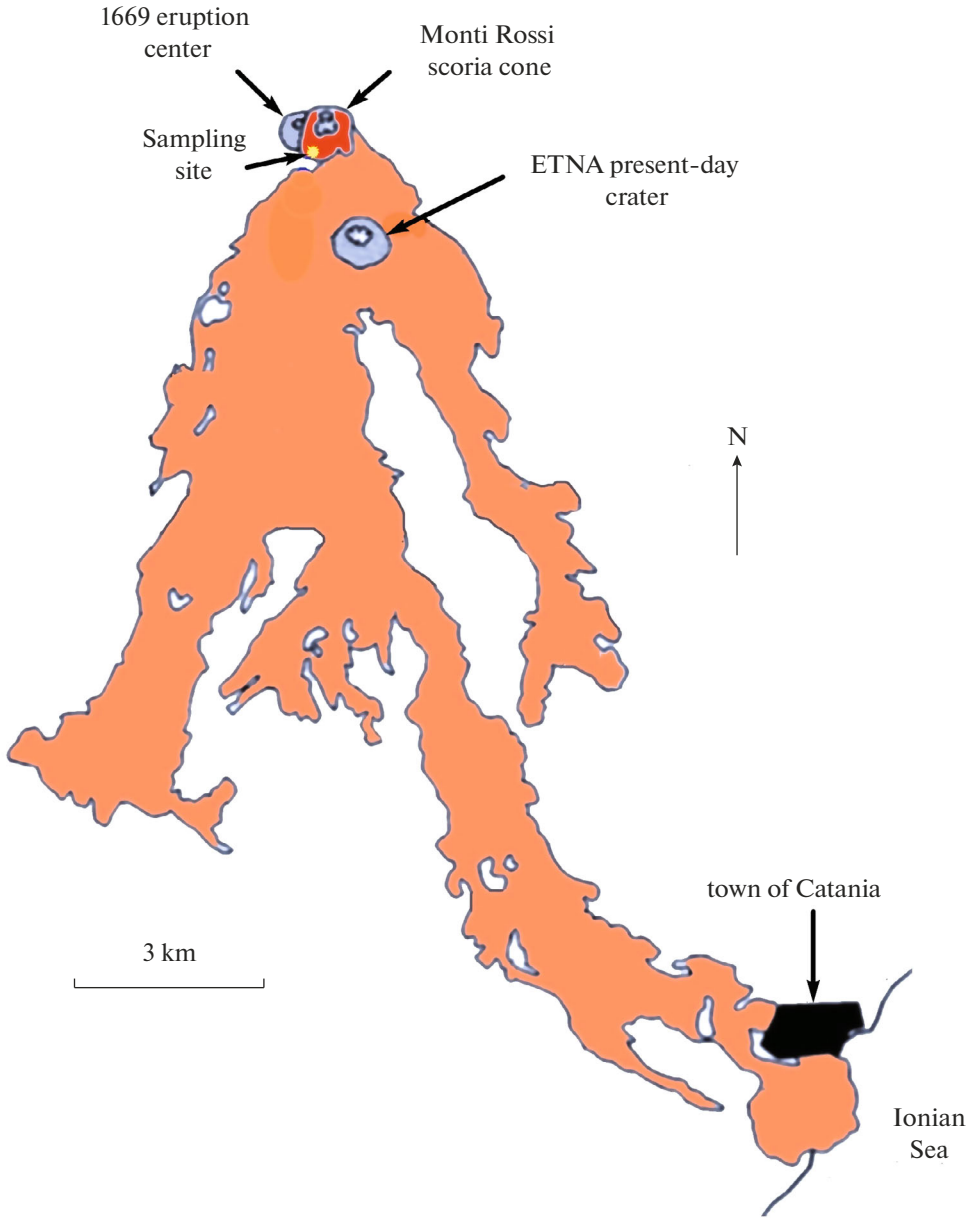

Fig. 4. A map of the scoria cone with the sampling site and lava flows (brown) due to the 1669 eruption.

TEPHRA GRAIN SIZE AND PARTICLE MORPHOLOGY

The grain-size analysis of the tephra was carried out by successively sieving the fractions and weighing afterwards. The results for two parts of the sample (A and B) turned out to be similar, showing a near normal 1D distribution of the particles in the range between 0.25 and 3 mm, i.e., from fine-grained psammites to gravel (Fig. 5). The mode of this distribution is at the fractions of coarse-grained psammites whose total percentage in the tephra is 73–75%. This character of the distribution and the obvious dominance of coarse-grained fractions provide convincing proof of near-crater location for the ash material studied.

The tephra particles show a nearly isometric aspect with the elongation index varying in the range 1.18 ± 0.08. The overwhelming majority of the particles have surfaces that are angular and flattened (Figs. 6a–6f) with occasional particles that are similar in size, but have smoothed and rounded surfaces (see Figs. 6g, 6h).

THE CHEMICAL COMPOSITION AND TRACE ELEMENTS

The effusive derivative lavas of the 1669 eruption, as reported by Italian researchers, vary in chemical composition from basalts and trachybasalts to basaltic trachyandesites, and further to trachydacites and tra-

Table 1. The bulk chemical composition of the tephra, wt %

Components	1	2	3	4	5	6	7	8	9	10	11	Mean ± RMS
SiO_2	44.96	45.41	44.86	44.67	43.90	44.52	45.14	45.18	44.57	43.79	44.37	44.67 ± 0.51
TiO_2	1.42	1.43	1.43	1.27	1.06	1.17	1.54	1.43	1.41	1.16	1.11	1.31 ± 0.16
ZrO_2	0.06	0.05	0.06	0.06	0.05	0.05	0.06	0.06	0.06	0.05	0.05	0.06 ± 0.01
Al_2O_3	19.58	18.08	18.48	19.45	18.60	18.09	18.79	19.35	19.39	19.25	19.10	18.92 ± 0.54
Cr_2O_3	0.02	N.d.	0.04	0.03	0.03	N.d.	N.d.	0.03	N.d.	0.03	0.03	0.02 ± 0.01
Fe_2O_3	10.76	11.49	10.78	10.72	10.72	10.29	10.80	10.88	10.85	10.85	10.72	10.81 ± 0.28
CuO	0.03	N.d.	0.03	0.02	0.02	0.02	0.03	0.03	0.02	0.02	0.02	0.02 ± 0.01
ZnO	0.02	"	0.02	0.02	0.01	0.01	0.02	0.02	0.02	0.02	0.01	0.02 ± 0.01
MnO	0.22	0.27	0.23	0.21	0.22	0.20	0.23	0.21	0.21	0.21	0.20	0.22 ± 0.02
MgO	4.38	3.95	4.53	6.06	8.55	7.33	4.43	4.54	5.23	7.65	7.64	5.84 ± 1.66
CaO	11.60	12.56	12.77	11.29	11.48	12.78	12.12	11.44	11.58	11.35	11.26	11.84 ± 0.6
SrO	0.13	0.12	0.12	0.12	0.11	0.11	0.12	0.12	0.13	0.11	0.12	0.12 ± 0.01
Na_2O	3.36	3.06	3.19	3.09	2.82	2.91	3.19	3.36	3.32	2.90	2.81	3.09 ± 0.21
K_2O	2.63	2.72	2.60	2.24	1.81	1.90	2.64	2.53	2.43	1.97	1.95	2.31 ± 0.35
Nb_2O_5	N.d.	N.d.	N.d.	0.01	N.d.	N.d.	N.d.	0.01	N.d.	N.d.	N.d.	0.001±0.004
P_2O_5	0.64	0.70	0.63	0.56	0.46	0.47	0.66	0.61	0.58	0.48	0.47	0.57 ± 0.09
SO_3	0.19	0.16	0.09	0.05	0.05	0.04	0.09	0.06	0.06	0.04	0.03	0.08 ± 0.05
Cl	N.d.	N.d.	0.14	0.13	0.11	0.11	0.14	0.14	0.14	0.12	0.11	0.11 ± 0.04

The data from X-ray fluorescence analysis have been normalized to 100%. RMS stands for root mean square deviation.

chytes (Fig. 7). Trachybasalts and basaltic trachyandesites are the most frequent rocks in the lavas. The tephra is obviously more basic than the lavas, varying in bulk composition from alkaline picrobasalts to alkaline basalts, only sporadically reaching trachybasalts (see Fig. 7, Table 1). Overall, these are alkaline basalts.

The volcanic glass occurring in the tephra (see Fig. 7, Table 2) varies in composition from alkaline picrobasalts to basalts, trachybasalts and alkaline basalts, and further to basaltic andesites and basaltic trachyandesites, with the average being trachybasalts.

The tephra was found to contain 50 trace elements, including 14 lanthanoids (Table 3). The concentrations of trace elements vary in very short ranges, as indicated by the values of the respective coefficients of variation that are in the range 9–50%. The total concentrations of trace elements vary between 1730 and 2350 (1985.28 ± 207.71) g/t, the total lanthanoids are 189–261 (223.24 ± 31.76) g/t. The Th–Hf–Ta (Wood, 1980), Ta/Nb–Th/Yb (Boynton, 1984), and Zr–Zr/Y diagrams show the data points for the tephra in the fields of the rocks that were generated under intraplate geodynamic settings. The Th/Yb–Nb/Yb diagram (Humbert et al., 2019) has the same points clustering between the values of primitive mantle and enriched MOR basalts.

The trends of indicator trace element concentrations as normalized by normal crust (Fig. 8a) correspond to those for trace elements in intraplate basaltoids. There is one important fact here, namely, relative enrichment of the tephra in niobium, strontium, titanium, and especially ytterbium. Our studies showed that the positive anomaly of ytterbium is indeed a direct indicator of the depth origin for material in the Earth's interior (Silaev et al., 2016).

The trend of chondrite-normalized lanthanoid concentrations is complementary to the corresponding trend for lanthanoid-enriched cerium E-MORB subgroup (see Fig. 8b). The general diagram of the N-Morb-normalized concentrations (see Fig. 8c) indicates an intraplate plume origin of the magmatism.

Comparative analysis suggests that the tephra discharged by the Etnean eruption under discussion is a product of melting in the deepest mantle regarded within the framework of examples of intraplate magmatism. The negative anomalies of Ti, Ni, and Cr are most likely due to accumulation of water in an intermediate chamber during magmatic differentiation, with magnetite, olivine, pyroxene, and basic plagioclase crystallized from the melt. It is noteworthy that the plots in Fig. 8c do not suggest a hint of a negative Ta–Nb anomaly, which provides evidence, not only of the absence of a subduction component in the region of magma generation, but also of an absence of a thick continental crust throughout the path of the ascending melt. Overall, our plots based on the tephra

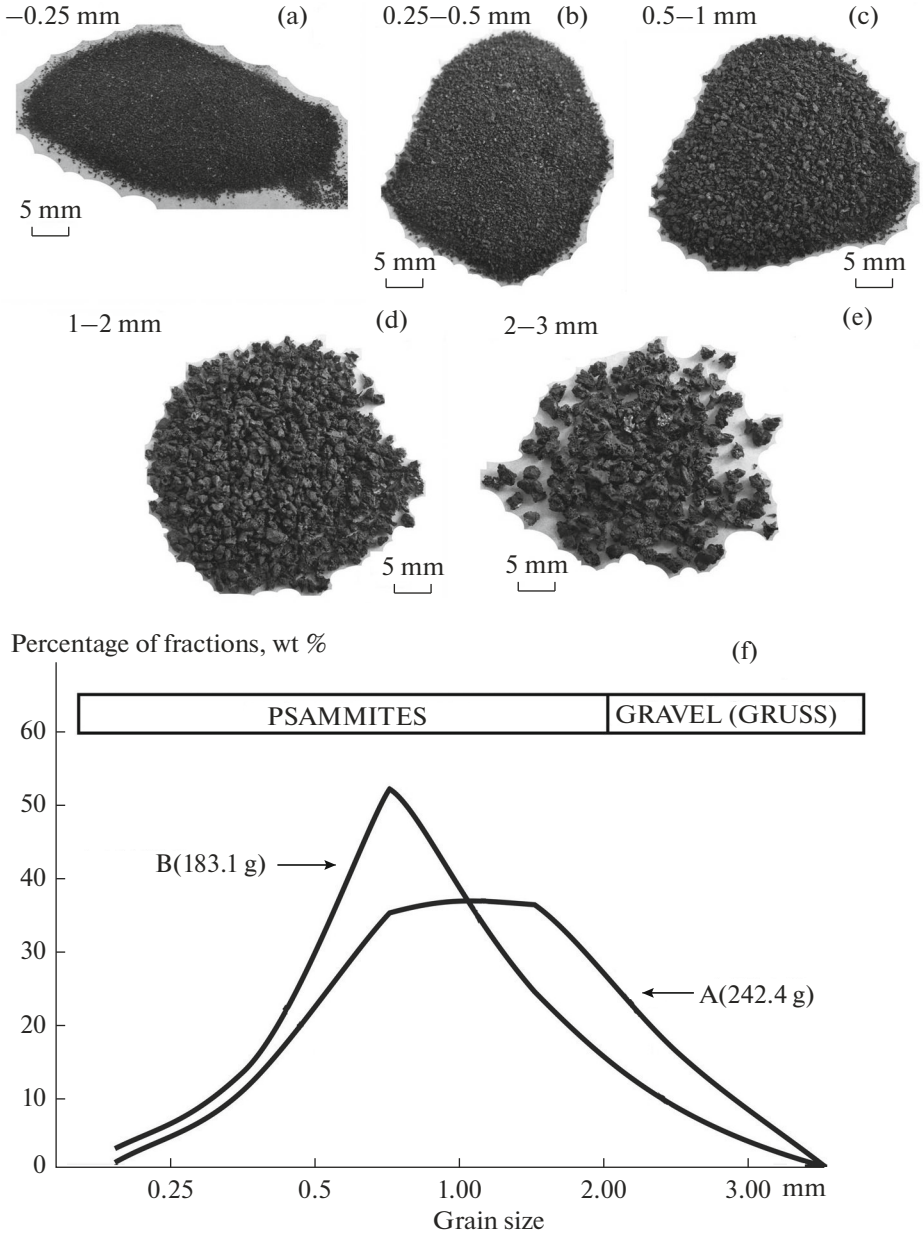

Fig. 5. The grain-size composition of the tephra. (a–e) grain-size fractions; (f) distribution of tephra particles over grain-size fractions; A and B mark the samples analyzed.

under study here can serve as a standard for products of deep-seated intraplate magmatism especially.

THE PHASE COMPOSITION AND TYPOMORPHIC MINERAL IN TEPHRA

The X-ray diffractograms of the tephra studied here show an amorphous halo (FWHM = 16°) in the angle range 2Θ 22°–38°, with maximum diffraction reflection occurring at 29°, which is appropriate to volcanic glass. Upon the background of this halo is a series of narrow peaks corresponding to microlites of rock-forming minerals; the proportions among these can be inferred from the number and intensities of the relevant reflections (in the order of decreasing relative concentrations).

Plagioclase with basic compositions was diagnosed in 34 reflections (Å, the relevant Miller indices are in parentheses): 4.04 (201)–3.90 ($1\bar{1}1$)–3.76 ($\bar{1}30$)–3.63 (130)–3.48 ($\bar{1}\bar{1}2$)–3.21 ($\bar{2}20$)–3.18 (002)–3.13 (220)–3.02 ($1\bar{3}1$)–2.94 ($0\bar{4}1$)–2.90 ($\bar{2}\bar{2}2$)–2.83 (131)–2.65 ($\bar{1}32$)–2.52 ($2\bar{2}1$)–2.46 ($\bar{2}40$)–2.27 ($\bar{3}\bar{3}1$)–2.13 ($2\bar{4}1$)–2.10 (151)–1.985 (061)–1.95 ($2\bar{2}2$)–1.929 ($4\bar{2}\bar{2}$)–1.881 ($\bar{2}60$)–1.849 ($\bar{4}03$)–1.835

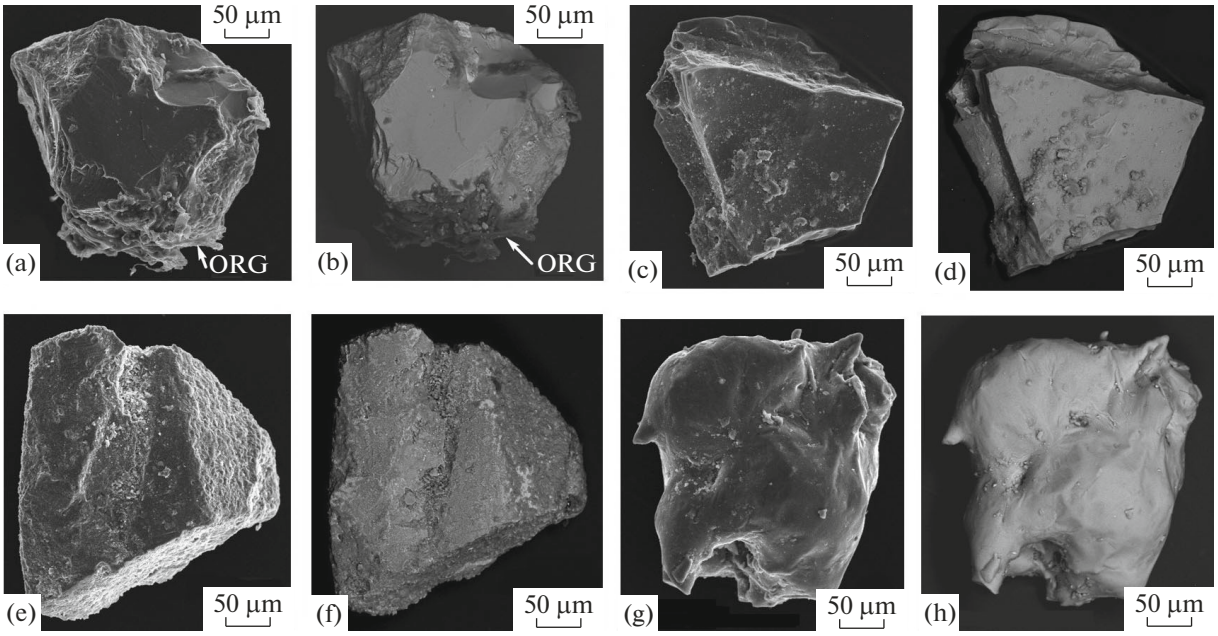

Fig. 6. The morphology of typical tephra particles. (a, b) shown are gouges of organoid particles (ORG); SEM images in secondary (a, c, e, g) and elastically reflected (b, d, f, h) electrons.

(0$\bar{6}$2)–1.816 (260)–1.798 ($\bar{1}$70)–1.772 ($\bar{2}$04)–1.756 (2$\bar{4}$2)–1.747 (420)–1.730 ($\bar{2}$24)–1.712 ($\bar{4}$41)–1.615 (353)–1.577 (0$\bar{2}$4).

Clinopyroxene (diopside) has been detected in 20 reflections: 4.67 (200)–3.24 (220)–2.99 (22$\bar{1}$)–2.94 (310)–2.90 (31$\bar{1}$)–2.56 (13$\bar{1}$)–2.52 (002)–2.22 (113)–2.13 (33$\bar{1}$)–2.10 (42$\bar{1}$)–2.04 (041)–2.02 (40$\bar{2}$)–1.835 (510)–1.816 (132)–1.756 (2$\bar{4}$2)–1.678 (042)–1.669 (31$\bar{3}$)–1.625 (22$\bar{3}$)–1.584 (530)–1.559 (600).

Quartz (9 reflections): 4.25 (100)–3.35 (101)–2.46 (110)–2.27 (102)–2.22 (111)–2.13 (200)–1.985 (201)–1.985 (201)–1.816 (112)–1.678 (202).

Olivine (5 reflections): 5.13 (020)–3.90 (021)–2.78 (130)–2.52 (112)–2.27 (233).

X-ray spectral microprobe method was applied to the tephra under study here to confirm the presence of the following minerals.

Olivine mostly corresponds to the composition of forsterite, occasionally of forsterite–hortonolite and hortonolite (Table 4). The empirical brutto formula of this mineral can be represented as $(Mg_{1.29–1.72}Fe_{0.30–0.69}Mn_{0–0.02})_{1.98–2.03}[SiO_4]$ or as $Fo_{65–86}$. It is this olivine which occurs in MORB and OIB basalts.

Magnetite is characterized by moderate titanium concentrations (Table 5), its brutto formula is $(Fe_{0.97–1}Mn_{0–0.03})(Fe_{1.55–1.88}Ti_{0.12–0.45}Cr_{0–0.05}V_{0–0.02})_2O_4$. Correlation analysis showed that the endmembers contained in the magnetite clearly divide (with pairwise correlation coefficients of ± 0.35–0.99) into two sets, the more dense ones (magnetite + chromite) and the less dense (ulvite + jacobsite + coulsonite). This indicates that pressure was probably one important factor favoring the crystallization of magnetite in the tephra under study here. That is to say, magnetite began to crystallize at great depths (relative enrichment in denser endmembers), and the process continued throughout the travel of the melt to the ground surface (enrichment in less dense endmembers).

The microminerals whose individuals measure (1.74 ± 0.68) × (1.14 ± 0.55) μm in the tephra include *rutile* $(Ti_{0.99–1}V_{0–0.01})O_2$, *monazite* $(La_{0.23–0.29}Ce_{0.45–0.52}Pr_{0.06–0.2}Nd_{0–0.2}Sm_{0–0.03}Gd_{0–0.03})[(P_{0.95–1}S_{0–0.05}O_4]$, *yarrowite-spioncopite* (the chalcosine group) $Cu_{1.28–1.3}S$, *native iron* $Fe_{0.9–0.93}Cu_{0.06–0.08}Zn_{0–0.01}Mn_{0–0.01})$, and *brass* $Cu_{0.59}Zn_{0.41}$. The locations where these occur on the surface of tephra particles, in particular, frequent occurrence in hollows and microcracks (Fig. 9), would suggest the inference that these minerals were formed in a gas–ash cloud during some later phase of the eruption. It should be noted that minerals such as these, namely, typically explosive ones, were also identified in discharges of Kamchatka volcanoes (Karpov et al., 2017; Silaev et al., 2019b).

LITHOGENIC GASES

The lithogenic gases that were encapsulated in the tephra were analyzed by gas chromatography (GC-17A Shimadzu chromatograph) using four-step heating in the range of temperatures 100–1000°C. The

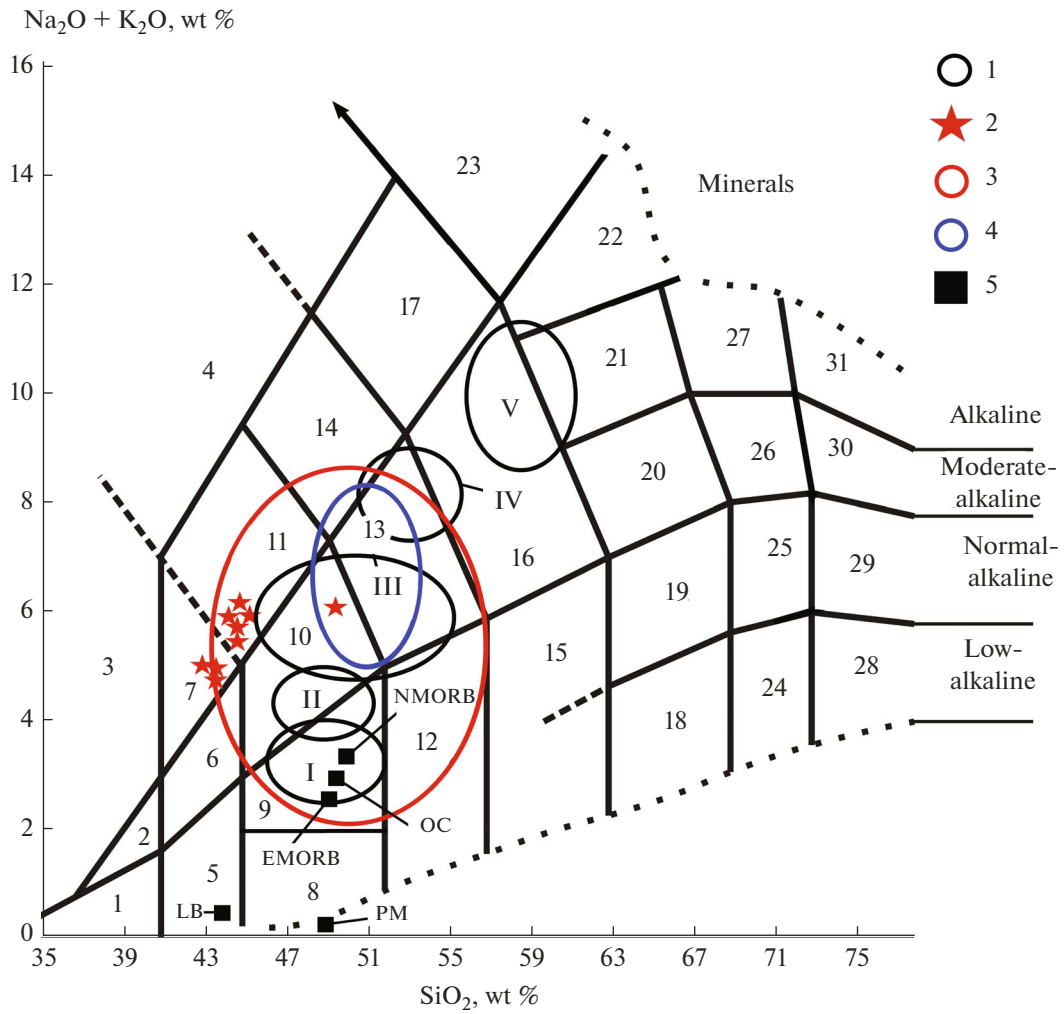

Fig. 7. A TAS diagram (Petrograficheski kodeks, 2008) for the chemistry of products from effusive (1) and explosive (2–4) facies of the 1669 Etna eruption. Graphs in the diagram: (1) picrites; (2, 3) picrites, moderately alkaline, alkaline, and basic, respectively; (4) fondites; (5–8) picrobasalts, ultrabasic, moderately alkaline, alkaline, and basic, respectively; (9) basalts; (10) trachybasalts; (11) alkaline basalts; (12) basaltic andesites; (13) basaltic trachyandesites; (14) phonotephrites; (15) andesites; (16) trachydacites; (17) tephriphonolites; (18) low alkali dacites; (19) dacites; (20) trachydacites; (21) trachytes; (22) alkaline trachytes; (23) phonolites; (24) low alkali rhyodacites; (25) trachydacites; (26) trachyrhyodacites; (27) alkaline rhyodacites (pantellerites); (28) low alkali rhyolites; (29) rhyolites; (30) trachyrhyolites; (31) alkaline rhyolites (comendites). Fields of lava composition (mean ± RMS) for the 1669 discharges (1): I basalts, II alkaline basalts, III trachybasalt–basaltic trachyandesite, IV basaltic trachyandesites, V trachyandesite-trachyte. The tephra: (2) data points of bulk composition, (3) field of volcanic glass in tephra particles, (4) composition of volcanic glass inclusions in organoid particles. Compositions of standard objects (5): LB lunar basalts, PM primitive mantle, N-MORB and E-MORB stand for normal and enriched MOR basalts, and OC stands for oceanic crust (Barsukov et al., 1979; Tarasov et al., 1980; Taylor and McLennan, 1985; Voitkevich et al., 1990).

procedures to be used in this analysis were worked out by us previously in multidisciplinary studies of Brazilian carbonado (Petrovsky et al., 2008). In the case under consideration, we analyzed four samples, with the results (Table 6) lending themselves to the following conclusions.

The composition of pyrolysates was due to two gas groups: (1) inorganic gases H_2, N_2, CO, CO_2, H_2O and (2) organic gases, namely, saturated and unsaturated hydrocarbons in the range C_1–C_4. The total concentration of gases that were released during heating varied between 2687 and 3758 μm/g, with the percentage of hydrocarbon gases being 6–11%. Gas release during heating showed a persistent tendency to decrease by factors of 1.8–4.3, which was ensured by decreases in the discharge of H_2O and N_2 by factors of 3–9 and 2–6, respectively. The concentrations of the other gases in the pyrolysates was increasing, reaching maxima for H_2, CO, and CO_2 at temperatures of 800–1000°C, while the hydrocarbon gases reached maxima in the range of temperatures 400–800°C. The lithogenic gases that were encapsulated in tephra particles thus contained progressively lesser amounts of (N_2 + H_2O) and greater amounts of H_2, CO, CO_2, and hydrocar-

Table 2. The chemical composition of volcanic glass in the tephra (1–10) and in organoids (11–17), wt %

##	SiO_2	TiO_2	Al_2O_3	Fe_2O_3	MnO	MgO	CaO	Na_2O	K_2O	P_2O_5	Cl
1	51.22	N.d.	28.04	1.07	N.d.	N.d.	11.89	7.27	0.51	N.d.	N.d.
2	49.33	2.44	15.18	11.93	″	3.89	6.56	4.86	4.61	0.83	0.37
3	49.27	1.86	14.98	10.69	″	6.18	7.02	6.10	2.55	1.35	N.d.
4	49.32	2.07	16.56	10.60	0.36	4.87	7.08	6.39	2.50	N.d.	0.25
5	46.27	2.54	12.06	20.80	N.d.	3.93	11.51	N.d.	3.19	″	N.d.
6	47.43	2.09	11.88	15.30	0.47	5.65	8.95	5.46	2.49	″	0.28
7	68.73	1.70	11.72	9.75	N.d.	3.26	3.82	N.d.	0.80	″	0.27
8	50.30	2.14	15.10	17.23	0.42	3.56	9.35	N.d.	1.90	″	N.d.
9	43.72	1.91	12.87	16.32	N.d.	5.97	9.90	5.35	2.95	1.01	″
10	46.06	2.34	13.90	19.74	0.71	4.29	0.46	N.d.	3.50	N.d.	″
Mean ± RMS	50.16 ± 6.90	1.91 ± 0.72	15.23 ± 4.79	13.34 ± 5.82	0.20 ± 0.27	4.16 ± 1.78	7.65 ± 3.51	3.54 ± 3.12	2.5 ± 1.21	0.32 ± 0.53	0.12 ± 0.15
11	49.88	2.61	16.20	13.63	N.d.	4.15	8.83	0.48	3.28	0.94	″
12	49.72	2.21	15.79	11.87	″	4.26	7.91	4.21	2.81	1.16	″
13	51.44	1.43	21.37	6.80	″	2.70	10.24	4.76	1.09	N.d.	0.17
14	51.53	1.43	21.41	6.81	″	2.70	10.25	4.77	1.10	″	N.d.
15	54.17	0.76	23.96	3.64	″	N.d.	9.59	6.27	1.61	″	″
16	55.10	H.o.	26.49	0.98	″	″	8.67	8.11	0.65	″	″
17	49.76	2.42	14.85	12.10	″	4.58	7.68	4.87	2.70	0.84	0.20
Mean ± RMS	51.66 ± 2.19	1.55 ± 0.95	20.01 ± 4.48	7.98 ± 4.74	N.d.	2.63 ± 1.94	9.02 ± 1.04	4.78 ± 2.31	1.89 ± 1.03	0.42 ± 0.53	0.05 ± 0.09

bons. From this it follows that it was the last gas group which was best preserved in tephra, hence had greater chances to have been primary.

Summarizing the data obtained (Fig. 10) suggested the following inference. Viewed from a petrologic standpoint, the compositions of both inorganic and organic lithogenic gases identified in the Etnean tephra is in obvious correlation with gas composition in products of crust–mantle interactions. We note that the emerging temperature trend in pyrolysate compositions only serves to intensify the affinity, indicating (for inorganic gases) the growth of CO and CO_2 relative to water in the high-temperature pyrolysates. As to the organic gases, one finds, first, the dominance of more complex hydrocarbons, which is the feature proper to deep-seated settings and, secondly, stepwise heating revealed the tendency of a significantly greater complexity in the composition of these gases due to mixing.

Overall, this study in the composition of lithogenic gases fully confirms a deep origin for the magma chamber that was the source of the tephra under study here, hence is consistent with the conclusion about an intraplate geodynamic origin of Mt. Etna.

ABIOGENIC ORGANOIDS

The tephra under study here was found to contain particles of black, optically opaque organoids that are encountered both as gouges to tephra particles (see Figs. 6a, 6b) and in a free state. Considered in relation to morphology and internal structure, these particles divide into two types, the fibrillar ones involving patches of clathrate structure and the globular lenticular ones.

The organoids of the first type (Fig. 11) are by far the most abundant. Their size varies in the range (456 ± 252) × (231 ± 136) μm (V = 55–60%). The elongation index is 2.47 ± 1.16 (V = 47%). The fibrils in the particles are 6.7 ± 7.8 μm thick (V = 116%). Consequently, the number of fibrils in a particle is 30–40 on average.

The organoids of the second type (Fig. 12) are more frequently observed as gouges to fibrillar particles (see Figs. 11a, 11b). They have rounded shapes with a characteristic convexity in the middle, their size is (47 ± 5.3) × (31.5 ± 7.4) × (9.3 ± 2.1) μm (V = 11–23%). The elongation index is 1.57 ± 0.28 μm (V = 23%).

Both types are saturated with minute inclusions of volcanic glass that has a composition similar to the glass in the tephra particles. The inclusions in the particles of fibrillar organoids vary in the range (10.9 ±

Table 3. Trace element concentrations in tephra, g/t

Elements	1	2	3	4	5	6	Mean ± RMS
Li	9	8	8	8	7	6	7.67 ± 1.03
Be	1.4	1.5	1.4	1.3	1.2	1.1	1.32 ± 0.15
B	6	4	6	3.6	3.4	2.8	4.3 ± 1.37
Sc	20	19	18	19	20	24	20 ± 2.1
V	280	200	160	200	150	190	196.67 ± 45.9
Cr	28	37	50	70	60	60	50.83 ± 15.8
Mn	1600	900	900	1000	900	1000	1050 ± 273.86
Co	30	29	30	42	42	50	37.17 ± 8.73
Ni	16	18	22	40	40	50	31 ± 14.13
Cu	120	120	120	110	100	90	110 ± 12.65
Zn	70	100	100	100	90	90	91.67 ± 11.69
Ga	17	18	18	17	16	15	16.83 ± 1.17
Ge	0.9	0.8	0.9	0.8	0.9	0.8	0.85 ± 0.05
As	2	1.7	1.5	1.24	1.22	1.1	1.46 ± 0.34
Se	0.63	0.84	0.59	0.58	0.5	0.65	0.63 ± 0.11
Rb	76	36	35	31	28	25	38.5 ± 18.83
Sr	1000	900	900	900	800	800	883.33 ± 75.28
Y	27	24	23	21	20	20	22.5 ± 2.74
Zr	270	220	210	190	180	170	206.67 ± 36.15
Nb	70	60	60	55	50	46	56.83 ± 8.49
Mo	6	3.5	3.4	3.1	2.8	2.5	3.55 ± 1.26
Ag	1.9	1.2	1.2	1	0.92	0.88	1.18 ± 0.38
Cd	0.13	0.17	0.14	0.14	0.14	0.13	0.14 ± 0.01
Sn	1.3	1.3	1.3	1.1	1	1	1.17 ± 0.15
Sb	0.13	0.12	0.13	0.1	0.09	0.09	0.11 ± 0.02
Te	0.21	0.01	0.01	0.01	0.01	0.01	0.04 ± 0.08
Cs	0.7	0.6	0.06	0.5	0.46	0.42	0.46 ± 0.22
Ba	600	500	500	480	430	400	485 ± 69.21
La	60	60	50	50	40	40	50 ± 8.94
Ce	110	110	90	90	80	80	93.33 ± 13.66
Pr	12	12	12	11	10	9	11 ± 1.26
Nd	50	50	40	40	38	36	42.33 ± 6.12
Sm	8	8	8	7	7	7	7.5 ± 0.55
Eu	2.3	2.4	2.3	2.2	2	2	2.2 ± 0.17
Gd	7	7	7	6	6	6	6.5 ± 0.55
Tb	0.8	0.8	0.8	0.7	0.7	0.7	0.75 ± 0.05
Dy	5	5	4.5	4.2	3.9	3.9	4.42 ± 0.5
Ho	0.9	0.9	0.8	0.8	0.7	0.7	0.8 ± 0.09
Er	2.4	2.3	2.2	2	1.9	1.8	2.1 ± 0.24
Tm	0.33	0.31	0.29	0.27	0.25	0.25	0.28 ± 0.03
Yb	2.1	1.9	1.8	1.7	1.56	1.5	1.76 ± 0.22
Lu	0.3	0.28	0.27	0.25	0.23	0.22	0.26 ± 0.03
Hf	5	4	4	4	4	4	4.17 ± 0.41
Ta	2.8	3.9	3.8	3.4	3	2.8	3.28 ± 0.49
W	0.9	0.6	0.7	0.5	0.5	0.4	0.6 ± 0.18
Tl	1.4	0.03	0.03	0.02	0.02	0.01	0.25 ± 0.56
Pb	7	8	12	5	6	4	7 ± 2.83
Bi	0.04	0.001	0.01	0.001	0.001	0.001	0.01 ± 0.01
Th	9	9	8	7	7	6	7.67 ± 1.21
U	2.5	2.4	2.4	2.1	2	1.8	2.2 ± 0.27

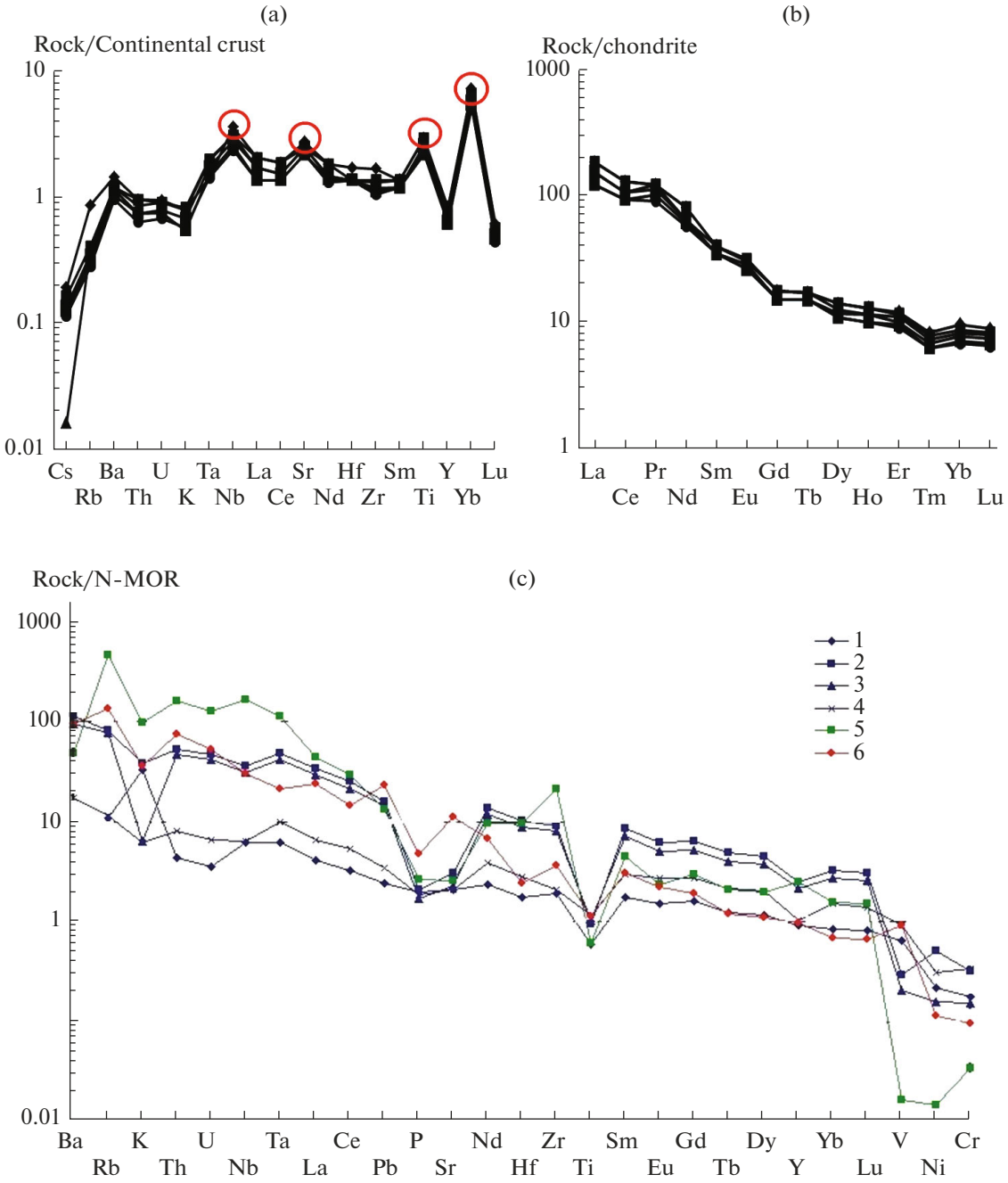

Fig. 8. Continental crust-normalized compositional trends for the most sensitive indicator trace elements in the tephra (in (a) we have marked the elements with abnormally high relative concentrations), chondrite (b), and N-MORB (c).

8.2) × (6.4 ± 4.7) μm, the elongation index is 2 ± 0.8. For the lenticular particles the same parameters are estimated as (4.8 ± 3.1) × (2.4 ± 1.3) μm and 2 ± 0.9. One finds some similarity in shape combined with some difference in the size of volcanogenic inclusions between the two types of organoid. The last evidently has direct correlation with particle size of the organoids themselves.

The chemical compositions of volcanic inclusions in different types of organoid particles are nearly identical, but the inclusions are compositionally variable within considerably narrow limits compared with the tephra glass, namely, ranging between alkaline basalts and basaltic andesites on the one hand and basaltic trachyandesites on the other, being generally consistent with the latter (see Fig. 7). Accordingly, the glass

Table 4. The chemical composition of olivine microlites in tephra, wt %

Components	1	2	3	4	5	6	Mean ± RMS
SiO_2	39.37	35.75	39.24	39.20	37.83	37.49	38.15 ± 1.42
Fe_2O_3	17.33	30.87	16.23	15.55	23.03	25.04	21.34 ± 6.05
MgO	43.30	30.85	43.88	44.87	38.77	36.98	39.78 ± 5.36
MnO	N.d.	0.53	0.45	0.38	0.37	0.49	0.44 ± 0.07

The data have been converted to 100%. The empirical formulas: (1) $(Mg_{1.65}Fe_{0.33})_{1.98}[SiO_4]$ (forsterite); (2) $(Mg_{1.29}Fe_{0.69}Mn_{0.01})_{1.99}[SiO_4]$ (hortonolite); (3) $(Mg_{1.68}Fe_{0.31}Mn_{0.01})_{1.99}[SiO_4]$ (forsterite); (4) $(Mg_{1.72}Fe_{0.30}Mn_{0.01})_{2.03}[SiO_4]$ (forsterite); (5) $(Mg_{1.54}Fe_{0.46}Mn_{0.01})_{2.01}[SiO_4]$ (forsterite); (6) $(Mg_{1.48}Fe_{0.50}Mn_{0.02})_2[SiO_4]$ (forsterite-hortonolite).

Table 5. The chemical composition of magnetite inclusions in tephra (1–5) and in organoids (6, 7), wt %

Components, wt %	1	2	3	4	5	6	7	Mean ± RMS
Fe_2O_3	84.81	96.08	91.65	90.79	90.96	84.97	88.49	89.58 ± 3.98
Cr_2O_3	N. d.	N. d.	1.27	1.28	1.71	N. d.	N. d.	0.61 ± 0.77
TiO_2	13.59	3.92	7.08	7.23	7.33	15.03	11.51	9.38 ± 4.04
MnO	0.83	N. d.	N. d.	0.70	N. d.	N. d.	N. d.	0.22 ± 0.37
V_2O_5	0.77	«	«	«	«	«	«	0.11 ± 0.29
Endmembers, mol %	1	2	3	4	5	6	7	Mean ± RMS
Magnetite $FeFe_2O_4$	55	88	77	76	75.5	55	65	70.21 ± 12.34
Ulvite Fe_2TiO_4	41	12	21	22	22	45	35	28.28 ± 12.13
Chromite $FeCr_2O_4$	N. d.	N. d.	2	2	2.5	N. d.	N. d.	0.93 ± 1.17
Jacobsite $MnFe_2O_4$	3	«	N. d.	N. d.	N. d.	«	«	0.43 ± 1.13
Coulsonite FeV_2O_4	1	«	«	«	«	«	«	0.14 ± 0.38

The data have been converted to 100%. The empirical formulas: (1) $(Fe_{0.97}Mn_{0.03})(Fe_{1.57}Ti_{0.41}V_{0.02})_2O_4$; (2) $Fe(Fe_{1.88}Ti_{0.12})_2O_4$; (3) $Fe(Fe_{1.75}Ti_{0.21}Cr_{0.04})_2O_4$; (4) $(Fe_{0.98}Mn_{0.02})(Fe_{1.74}Ti_{0.22}Cr_{0.04})_2O_4$; (5) $Fe(Fe_{1.73}Ti_{0.22}Cr_{0.05})O_4$; (6) $Fe(Fe_{1.55}Ti_{0.45})O_4$; (7) $Fe(Fe_{1.65}Ti_{0.35})_2O_4$.

of these inclusions contains somewhat more of Al_2O_3, CaO, Na_2O, but less of MgO and Fe_2O_3. In addition, it transpired that the volcanic glass contained in organoids is more homogeneous than that in tephra particles themselves, judging from many rock-forming components (SiO_2, Al_2O_3, CaO, Na_2O, and P_2O_5). The pattern is reversed, when we consider the other components (TiO_2, Fe_2O_3, MgO). An analysis of organoids proper indicated a considerable admixture of inorganic components (wt %): SiO_2 3.75 ± 3.66; TiO_2 0.09 ± 0.19; Al_2O_3 1.79 ± 1.66; Fe_2O_3 1.12 ± 1.32; MgO 0.23 ± 0.39; CaO ± 3.11 ± 1.7; K_2O 0.41 ± 0.41; P_2O_5 0.22 ± 0.48; SO_3 0.78 ± 0.62; the total content is 11.49 ± 7.51. All of the main components of the admixture show strong positive correlations, $r = 0.42–0.96$. Evidently, the composition and correlations of the inorganic substance in organoids characterize it as a fine dispersed admixture of volcanogenic material.

The phase diagnostics of organoids was performed by E.A. Vasiliev (Mining University, St. Petersburg) using Raman spectroscopy. Unlike the strongly luminescent substance of the present-day vegetable and animal organic matter (Silaev et al., 2013), the organoids studied here produce RS-spectra with two considerably broader Raman lines upon the background of moderate luminescence peaking at 1410–1435 cm^{-1} (FWHM = 150–170 cm^{-1}) and 1580–1600 cm^{-1} (FWHM = 100–110 cm^{-1}), which have positions close to the lines in spectra of many carbonaceous substances, D (A_{1g} is the mode of oscillation for carbon atoms) and G (E_{2g} is the mode). Spectra such as these are usually interpreted as resulting from scattering at aromatic rings and at chemical bonds C=O.

The elemental composition of the organoids was analyzed using a Tescan VEGA 3 analytical SEM with an X-max50 ED spectrometer (wt %): C = 62.86 ± 7.48; N = 16.07 ± 1.15; O = 21.07 ± 8.34. These results are rather similar to those obtained previously for particles of condensed organoids in discharges of Kamchatka volcanoes (Silaev et al., 2018a, 2018b; 2019a). Modern bacteria when studied using the same method and the same instrument gave a result that differs significantly from that for organoids (wt %): C = 78.73 ± 4.79; N = 11.41 ± 4.66; O = 9.85 ± 2.61 wt %. In addition, compared with the organoids identified in the

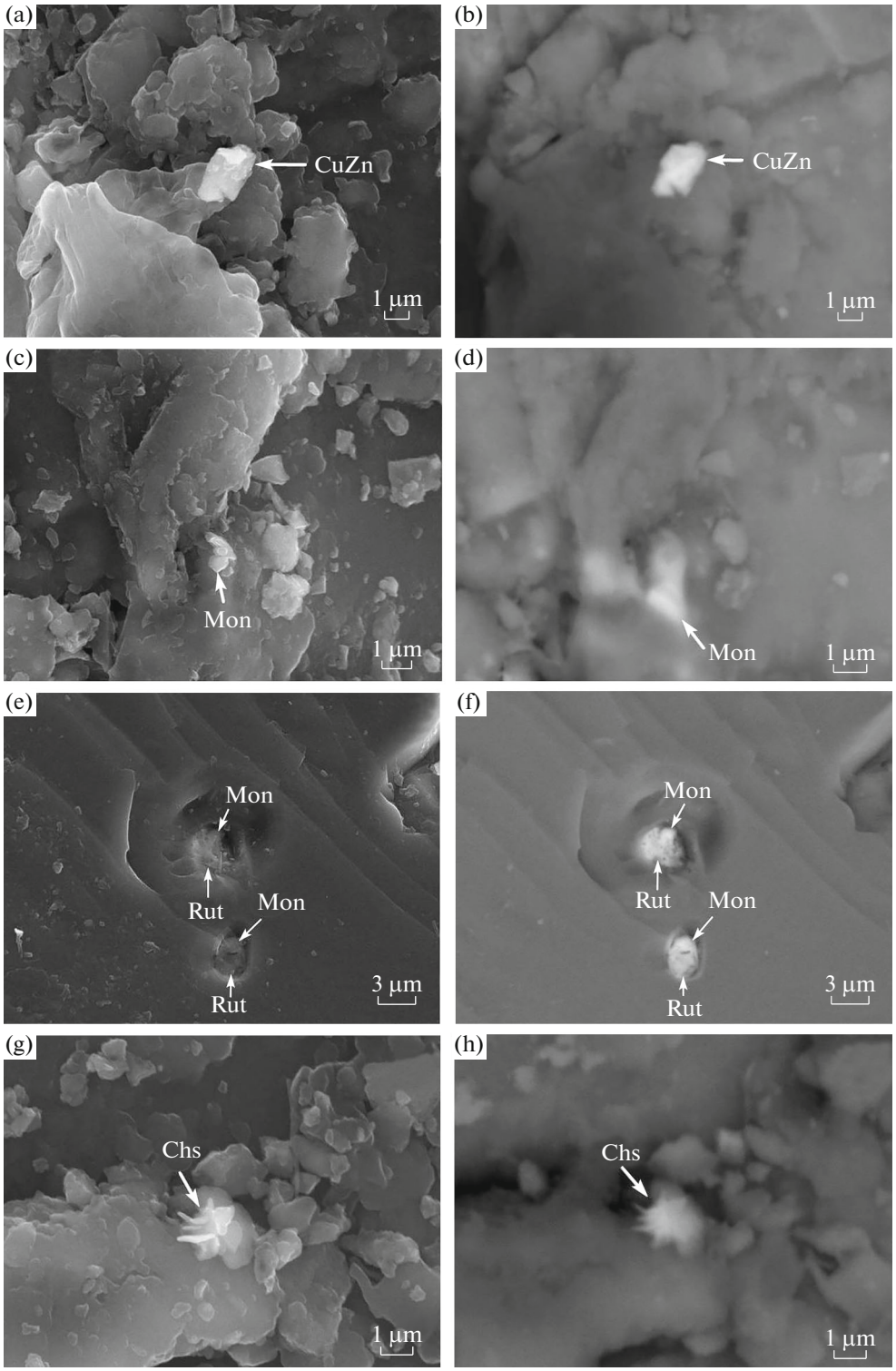

Fig. 9. Accessory elements in the tephra. CuZn brass, Mon monazite, Rut rutile, Chs stands for yarrowite–spioncopite. SEM images in secondary (a, c, e, g) and elastically reflected (b, d, f, h) electrons.

Etnean tephra, the bacteria turned out to be much more homogeneous by carbon concentration (the coefficient of variation was 6 against 12%) and oxygen concentration (26 against 40%).

Judging from the isotope composition of carbon and nitrogen, the organoids are similar to the carbonaceous material that is dispersed in the Etnean tephra itself (Table 7), thus indicating a genetic affinity

Table 6. The chemical composition of pyrolysates obtained by stepwise heating of tephra samples

Sample no.	T, °C	H_2	N_2	CO	CO_2	H_2O	CH_4	C_2H_4	C_2H_6	C_3H_6	C_3H_8	Total
1/1	100–400	0	12.9	56.22	101.57	1645	0.135	0.075	0.002	0.125	0.023	1816.05
			0.71	3.1	5.59	90.58	0.007	0.004	0.0001	0.007	0.002	100
1/2	400–600	0.55	3.04	43.31	267.39	661	6.157	4.339	2.248	6.02	2.384	996.438
		0.055	0.305	4.35	26.838	66.336	0.618	0.435	0.226	0.6	0.237	100
1/3	600–800	207	1.68	24.26	122.55	364	9.01	3.245	2.177	3.312	1.291	533.595
		0.388	0.315	4.546	22.967	68.216	1.688	0.608	0.408	0.621	0.242	100
1/4	800–1000	1.3	2.34	40.1	166	189	1.269	0.064	0.009	0.011	0.003	411.796
		3.157	0.568	9.738	40.311	45.896	0.308	0.015	0.002	0.003	0.002	100
2/1	100–400	0	6.5	15.59	68.58	1043	0.041	0.042	0.001	0.111	0.024	1133.889
			0.573	1.375	6.048	91.984	0.004	0.004	0.0001	0.01	0.09	100
2/2	400–600	0.71	1.03	43.6	268.65	840	5.859	4.456	2.441	5.798	2.25	1174.794
		0.06	0.088	3.711	22.868	71.502	0.499	0.379	0.208	0.493	0.192	100
2/3	600–800	1.3	0	13.98	77.35	131	7.869	4.015	2.881	4.08	1.554	244.029
		0.533		5.729	31.697	53.682	3.225	1.645	1.181	1.672	0.636	100
2/4	800–1000	7.47	3.46	74.03	607.68	360	4.985	0.538	0.156	0.221	0.038	1058.578
		0.706	0.327	6.993	57.405	34.008	0.471	0.051	0.015	0.021	0.003	100
3/1	100–400	0	4.56	13.53	50	865	0.044	0.029	0.004	0.064	0.002	933.253
			0.491	1.45	5.358	92.687	0.005	0.003	0.0004	0.006	0.0002	100
3/2	400–600	0.28	0.084	37.74	267.45	721	5.222	4.009	2.257	5.714	2.368	1046.88
		0.027	0.08	3.605	25.547	68.871	0.499	0.383	0.215	0.546	0.227	100
3/3	600–800	2.75	0	20.42	111.25	251	10.531	4.508	3.301	4.64	2.057	410.457
		0.67		4.97	27.104	61.151	2.566	1.098	0.804	1.13	0.507	100
3/4	800–1000	2.61	0	39.85	145.144	106	2.09	0.091	0.018	0.014	0	296
		0.881		13.457	49.116	35.797	0.706	0.031	0.006	0.006		100
4/1	100–400	0	7.29	39.56	52.95	795	0.074	0.026	0	0.071	0	894.971
			0.815	4.42	5.916	88.829	0.009	0.003		0.08		0
4/2	400–600	0	3.93	46.49	284.28	684	4.645	2.688	1.308	3.813	1.596	1032.75
			0.381	4.502	27.526	66.23	0.45	0.26	0.127	0.369	0.155	100
4/3	600–800	2.77	0	25.58	148.57	189	10.327	4.605	3.107	4.796	1.741	390.496
		0.709		6.551	38.046	48.4	2.644	1.179	0.796	1.228	0.447	100
4/4	800–1000	3.59	1.22	72.56	294.79	120	1.909	0.091	0.009	0.013	0	494.182
		0.726	0.247	14.683	59.652	24.282	0.386	0.018	0.002	0.004		100

The data for concentrations of components are in μm/g (top) and in % (bottom).

between them. Judging from isotope properties, both the tephra and the organoids can be correlated with the endogenous carbonaceous material present in the present-day MORs (Cartigny, 2005) and the carbon found in volcanics and volcanogenic organoids occurring in Kamchatka (Fig. 13). The present-day bacteria, microfungi, and microalgae are characterized by substantially different isotopic parameters (‰): 1) bacteria, $\delta^{13}C_{PDB} = -19.01 \pm 1.80$, $\delta^{15}N_{air} = 6.48 \pm 3.75$; 2) microfungi and microalgae, $\delta^{13}C_{PDB} = -15.65 \pm 1.35$, $\delta^{15}N_{air} = 1.57 \pm 1.37$.

We thus see that the RS spectra, elemental composition, the isotopy of carbon and nitrogen, all substan-

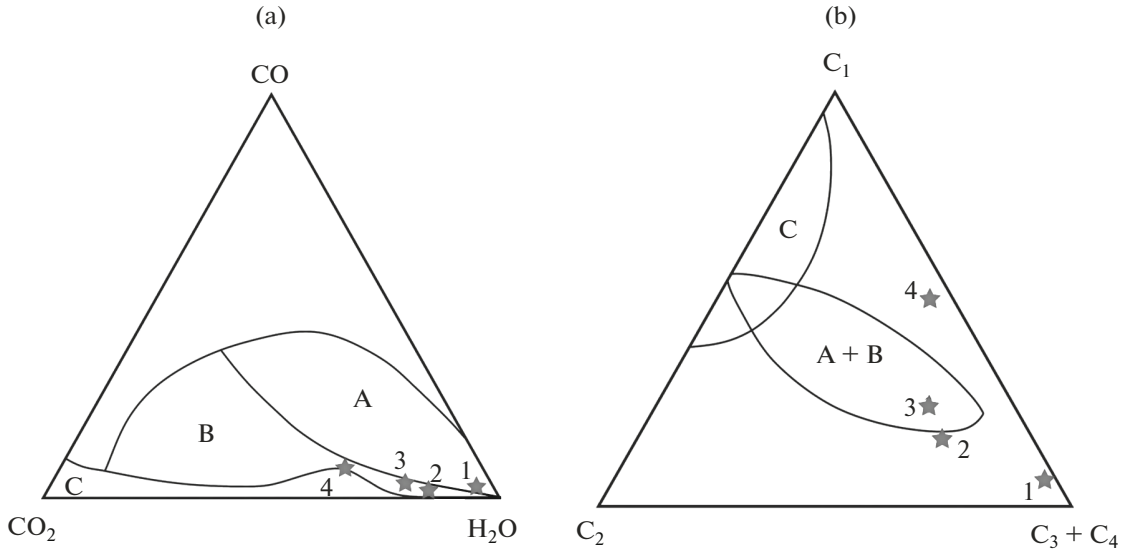

Fig. 10. Petrologic aspects in the generation of lithogenic gases in the tephra. (a) proportions of inorganic gases in mantle–crust derivates (A mantle derivates (diamonds), B products of mantle–crust interactions (minerals of diamond-bearing parastereses), C crustal derivates) (Petrovsky et al., 2008)); (b) same, for hydrocarbon gases (C_1 methane, C_2 ethane, $C_3 + C_4$ propane + butane). Stars show the compositions of pyrolysates obtained during heating in the ranges 100–400 (1), 400–600 (2), 600–800 (3), and 800–1000 (4)°C.

tially distinguish the organoids identified in the Etnean tephra from present-day organisms, and can safely be regarded as abiogenic derivates. The identification of such derivates on Mt. Etna confirms our previous inference concerning a global occurrence of carbon abiogenesis under the conditions of present-day volcanism.

CONCLUSIONS

This paper reports the first-ever multidisciplinary mineralogical and geochemical studies of the tephra discharged by the 1669 catastrophic eruption on Mt. Etna, Sicily, one of the most active volcanoes in the world. This tephra is characterized by coarse psammite grain-size composition, providing evidence of a near-crater location of the ash material. By bulk chemical composition, it varies between alkaline picrobasalts and trachybasalts, being more basic compared with the lavas of this eruption. The volcanic glass in the tephra varies in chemical composition in a slightly wider range, between alkaline picrobasalts and basaltic trachyandesites, thus indicating some degree of crystallization in tephra material.

The tephra was found to contain 50 trace elements whose total is 1985 ± 208 g/t. It follows from the Th–Hf–Ta, Ta/Nb–Th/Yb, and Zr–Zr/Y diagrams that the tephra is consistent with the volcanism under an intraplate geodynamic setting. The trends in the concentrations of indicator trace elements as normalized by continental crust are consistent with analogous trends in intraplate basaltoids. The relevant plots clearly reveal an ytterbium maximum, which indicates a considerable depth for the generation of magma material. Regarded with respect to the trend of chondrite-normalized lanthanoid concentrations, the Etnean tephra is complementary to E-MORB, with the general diagram for N-MORB-normalized concentrations indicating an intraplate plume origin of the magmatism. It thus appears that all geochemical data obtained for the tephra can safely be regarded as classifying Mt. Etna as an intraplate volcano with a deep magma chamber. It is not to be ruled out that the Etna data can serve as the standard for diagnostics of volcanoes that are active under an intraplate geodynamic setting.

The microlites in the tephra were found to contain olivine of the composition $Fo_{65–86}$, diopside, basic plagioclase, and occasional quartz. Also, there are inclusions of Cr–V-bearing ulvite-magnetite whose endmember composition shows that it began to crystallize at a considerable depth. The microminerals of explosive origin include rutile, yarrowite-spioncopite (the chalcosine group), native iron, and brass.

The inorganic and organic lithogenic gases identified in the Etnean tephra correlate with the composition of the gases found in products of crust–mantle interactions. The temperature-dependent trend of pyrolysate composition for inorganic gases indicates the growth of the role of CO and CO_2 in the deeper encapsulated fluid inclusions relative to water, while the analogous situation for organic gases indicates the dominance of hydrocarbons that are more complex compared with methane. This is a feature that is peculiar to deep settings.

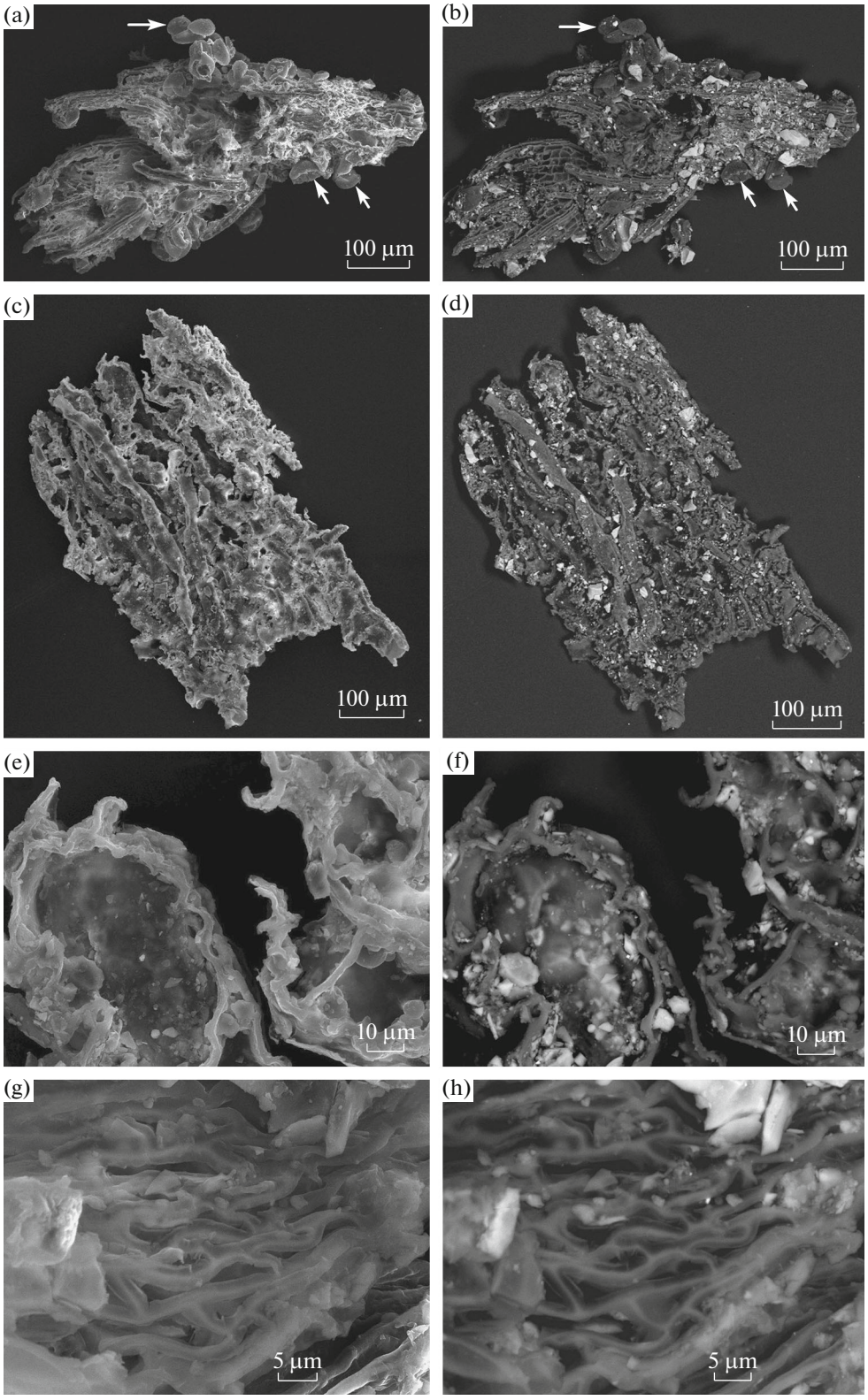

Fig. 11. The morphology of fibrillar organoids. Arrows in (a, b) mark organoid gouges of globular lenticular shapes; SEM images in secondary (a, c, e, g) and elastically reflected (b, d, f, g) electrons. Brighter particles in (b, d, f, g) are contaminations of organoids with volcanic ash microparticles.

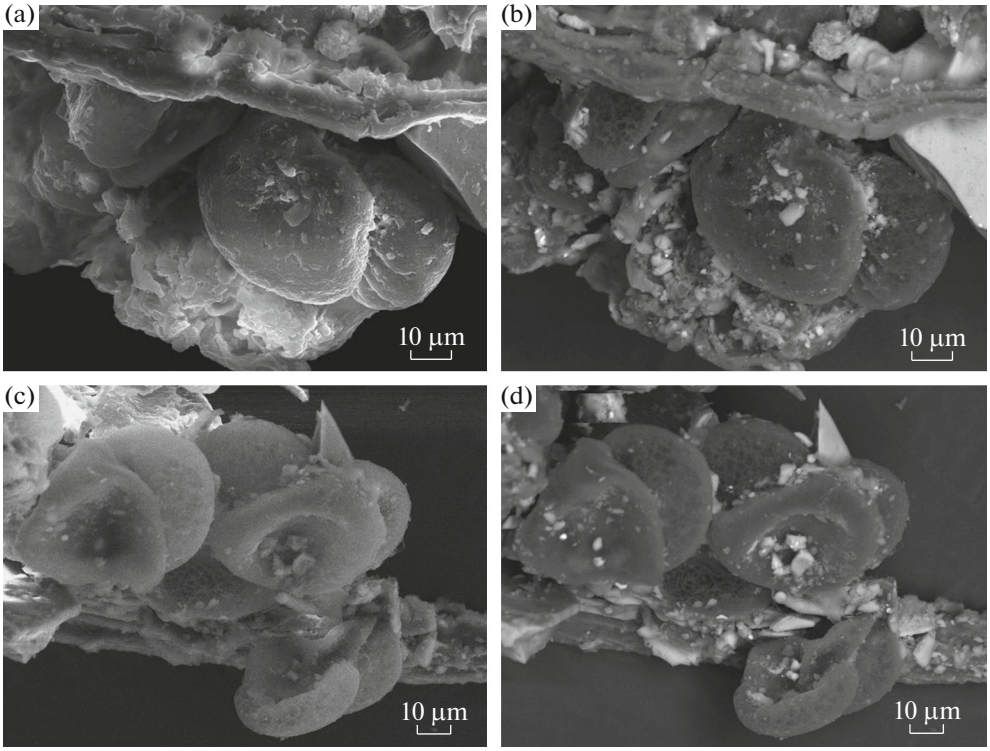

Fig. 12. The morphology of particles of globular lenticular organoids. SEM images in secondary (a, c) and in elastically reflected (b, d) electrons. Brighter particles in b, d are surface contaminations of organoids with volcanic material.

Table 7. The isotope composition of carbon and nitrogen in tephra (1–10) and in organoids (11–16), ‰

##	$\delta^{13}C_{PDB}$	$\delta^{15}N_{Air}$
1	–24.11	1.55
2	–27.72	
3	–27.74	
4	–27.88	
5	–27.1	
6	–27.57	
7	–27.9	
8	–27.46	
9	–27.77	
10	–27.26	
11	–27.42	
12	–27.4	
13	–27.25	
14	–27.23	
15	–27.5	
Statistic	–27.29 ± 0.91	
(mean ± RMS)	(V = 3.3%)	
16	–27.32	1.55
17	–25.15	1.2
18	–27.4	1.6
19	–25.13	1.5
20	–24.89	1.4
21	–23.64	1.3
Statistic	–25.59 ± 1.48	1.43 ± 0.15
(mean ± RMS)	(V = 5.8%)	(V = 10.5%)

The tephra under study here was found to contain particles of abiogenic organoids that divide into fibrillar and globular lenticular types by their morphology and internal structure. Both types of particles are saturated with a fine dispersed admixture and with minute inclusions of volcanic glass whose composition is similar to that of the glass in tephra particles, but which varies in considerably narrower limits, from alkaline basalts and basaltic andesites to basaltic trachyandesites. With regard to their phase and elemental composition, as well as the isotopy of carbon and nitrogen, the organoids detected in the Etnean tephra differ from present-day bacteria, microfungi, and microalgae, but are similar to abiogenic organoids found in products of Kamchatka volcanoes. The last circumstance corroborates our earlier inference about a global occurrence of carbon abiogenesis under the conditions of onshore volcanism.

FUNDING

The ICP-MS trace element analysis was performed at the *Geoanalitik* TsKP UrO RAN for the research topic no. AAAA-A18-118053090045-8 of the State Assignment at the Institute of Geology and Geochemistry, Ural Branch, Russian Academy of Sciences.

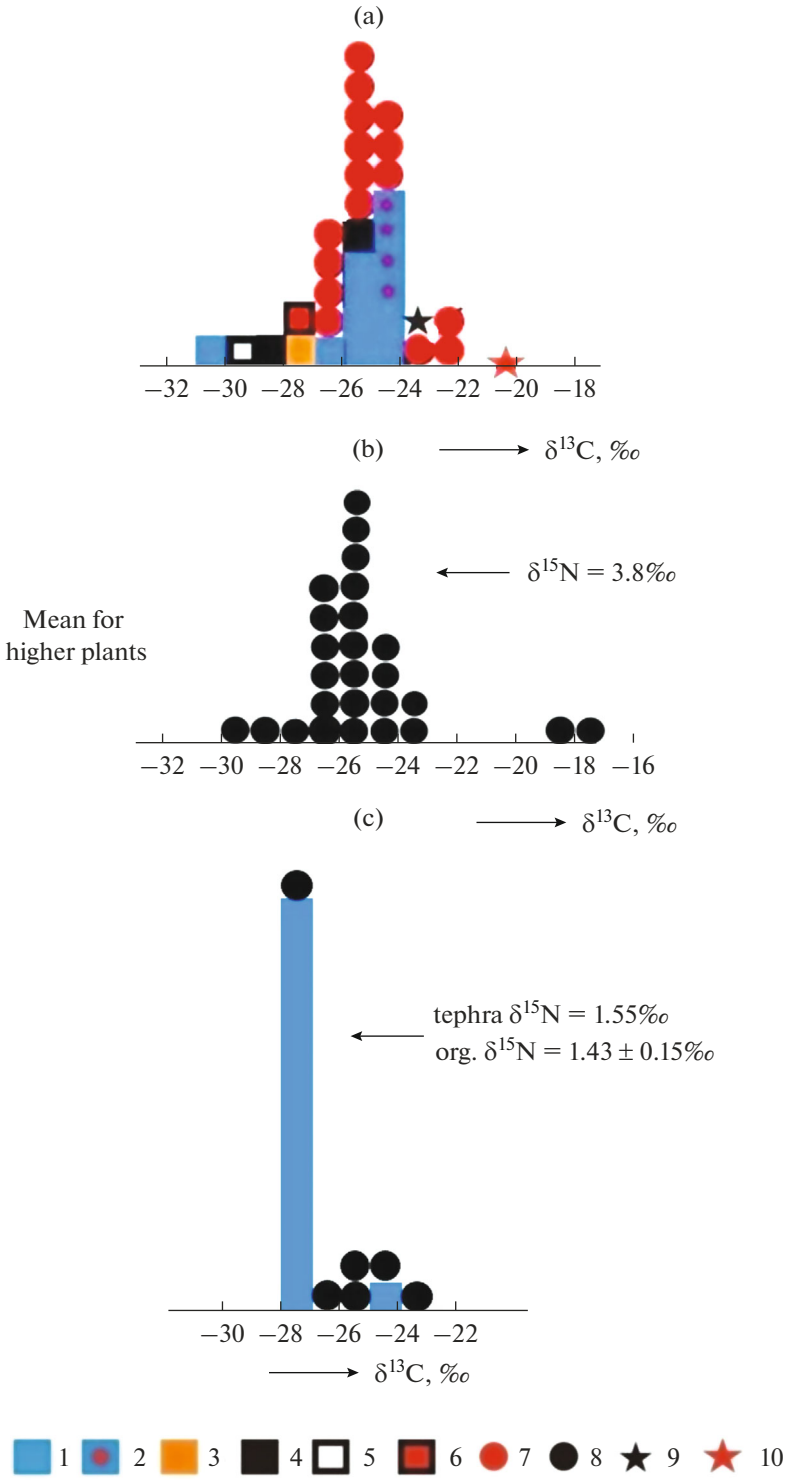

Fig. 13. The isotope composition of the carbon atom-dispersed in products of recent volcanism (a) and carbon and nitrogen in condensed volcanogenic organoids in Kamchatka (b), in tephra and organoids discharged by the 1669 Etna eruption (c). (1) lavas and ash of the TFE-50, Etnean tephra; (2, 3) diamond-bearing tephra discharged by the TFE-50 and by Klyuchevskoi; (4) bitumen-like HC from TFE-50 ashes; (5) bitumen-like HC containing inclusions of native aluminum from TFE-50 ashes; (6) particles of native aluminum with inclusions of microdiamonds, Klyuchevskoi Volcano; (7) Tolbachik diamonds; (8) organoids from Kamchatka volcanic ash and Etnean tephra; (9) dicarbon globules; (10) carbonaceous substance in meteorites.

REFERENCES

Barsukov, V.L., Nazarov, M.A., and Tarasov, L.S., The mineralogy of lunar material, *Zapiski VMO,* 1979, *Part* 108, no. 1, pp. 3–14.

Ben Avraham, Z., Boccaletti, M., Cello, G., Grasso, M., Lentini, F., Torelli, L., and Tortorici, L., Principali domini strutturali originatisi dalla collisione neogenico-quaternaria nel Mediterraneo central, *Mem. Soc. Geol. Ital.,* 1990, vol. 45, pp. 453–462.

Boynton, W.V., Geochemistry of the rare earth elements: Meteorite studies, in *Rare Earth Element Geochemistry,* Amsterdam: Elsevier, 1984, pp. 63–114.

Branca, S., Coltelli, M., Groppelli, G., and Lentini, F., Geological map of Etna volcano, 1:50000 scale, *Italian Journal of Geosciences,* 2011a, vol. 130(3), pp. 265–291. https://doi.org/10.3301/IJG.2011.15

Branca, S., Coltelli, M., and Groppelli, G., Geological evolution of a complex basaltic stratovolcano: Mount Etna, Italy, *Italian Journal of Geosciences,* 2011b, vol. 130(3), pp. 306–317. https://doi.org/10.3301/IJG.2011.13

Cartigny, P., Stable isotopes and the origin of diamond, *Elements,* 2005, vol. 1, pp. 79–84.

Chironi, C., De Luca, L., Guerra, I., et al., Sea land group crustal structures of the Southern Tyrrhenian Sea and Sicily Channel on the basis of the M25, M26, M28, M39, WARR profiles, *Bull. Della Soc. Geol. Italy,* 2000, vol. 119, pp. 189–203.

Correale, A., Scribano, V., and Paonita, A.A., Volcanological paradox in a thin-section: Large explosive eruptions of high-Mg magmas explained through a vein of silicate glass in a serpentinized peridotite xenolith (Hyblean area, Sicily), *Geosciences (MDPI),* 2019, vol. 9, pp. 150. https://doi.org/10.3390/geosciences9040150

Corsaro, R.A., Cristofolini, R., and Patanè, L., The 1669 eruption at Mount Etna: chronology, petrology and geochemistry, with inferences on the magma sources and ascent mechanisms, *Bull. Volcanol.,* 1996, vol. 58, pp. 348–358.

De Beni, E., Branca, S., Coltelli, M., et al., 39Ar/40Ar isotopic dating of Etna volcanic succession, *Italian Journal of Geosciences,* 2011, vol. 130(3), pp. 292–305. https://doi.org/10.3301/IJG.2011.14

Encyclopedia of Volcanoes, Sigurdsson, H., Houghton, B., Rymer H., Stix, J., and McNutt, S., Eds.,. Academic Press, 1999, pp. 1172–1177.

Finetti, I., Structure, stratigraphy and evolution of central Mediterranean, *Bull. Di Geofis. Teor. e Appl.,* 1982, vol. 24, pp. 247–312.

Giampiccolo, E., Brancato, A., Manuella, F.C., et al., New evidence for the serpentinization of the Palaeozoic basement of southeastern Sicily from joint 3D seismic velocity and attenuation tomography, *Geophys. J. Int.,* 2017, vol. 211, pp. 1375–1395.

Guest, J.E., Styles of eruption and flow morphology on Mt. Etna, *Memorie Società Geologica Italiana,* 1982, vol. 23, pp. 49–73.

Humbert, F., de Kock, M.O., Lenhardt, N., and Altermann, W., Neoarchaean to Early Palaeoproterozoic within-plate volcanism of the Kaapvaal Craton: Comparing the Venters-dorp Supergroup and Ongeluk and Hekpoort Formations (Tranvaal Supergroup), in *The Archaean Geology of the Kaapval Craton, Sonthern Africa,* Springer Nature Switzerland AG, 2019, pp. 277–302.

Karpov, G.A., Silaev, V.I., Anikin, L.P., et al., Explosive mineralization, in *Tolbachinskoe treshchinnoe izverzhenie 2012–2013 gg.* (The Tolbachik Fissure Eruption of 2012–2013), Novosibirsk: SO RAN, 2017, pp. 241–255.

Manuella, F.C., Scribano, V., Carbone, S., and Brancato, A., The Hyblean xenolith suite (Sicily): an unexpected legacy of the Ionian–Tethys realm, *Int. J. Earth Sci. (GR Geologische Rundschau),* 2015, vol. 104, pp. 317–1336.

Petrovsky, V.A., Silaev, V.I., Sukharev, A.E., et al., Fluid phases in carbonado and their genetic significance, *Geochemistry International,* 2008, vol. 46, no. 7, pp. 693–710.

Romano, R., Succession of the volcanic activity in the Etnean area, *Memorie Società Geologica Italiana,* 1982, vol. 23, pp. 27–48.

Scribano, V., Sapienza G., Braga, R., and Morten, L., Gabbroic xenoliths in tuff-breccia pipes from the Hyblean Plateau: Insights into the nature and composition of the lower crust underneath Southeastern Sicily, Italy, *Miner. Pet.,* 2006a, vol. 86, pp. 63–88.

Scribano, V., Ioppolo, S., and Censi, P., Chlorite/smectite-alkali feldspar metasomatic xenoliths from Hyblean Miocenic diatremes (Sicily, Italy): Evidence for early interaction between hydrothermal brines and ultramafic/mafic rocks at crustal levels, *Ofioliti,* 2006b, vol. 31, pp. 161–171.

Silaev, V.I., Lyutoev, V.P., Petrovsky, V.A., and Khazov, A.F., A study of naturally occurring carbonaceous substances and some of their synthetic analogues by the method of Raman spectroscopy, *Mineralog. Zhurn.,* 2013, vol. 35, no. 3, pp. 33–47.

Silaev, V.I., Proskurnin, V.F., Gavrish, A.V., et al., A carbonatite assemblage of unusual rocks and mineralizations in eastern Taimyr, in *Problemy mineralogii petrografii i metallogenii* (Problems in Mineralogy, Petrography, and metallogeny), Issue 19, Perm, 2016, pp. 119–136.

Silaev, V.I., Anikin, L.P., Shanina, S.N., et al., *Abiogennye kondensirovannye organicheskie polimery v produktakh sovremennogo vulkanizma v svyazi s problemoi vozniknoveniya zhizni na Zemle* (Abiogenic Condensed Organic Polymers in Ejecta of Recent Volcanism in Relation to the Origin of Life on Earth), Syktyvkar: Geoprint, 2018a.

Silaev, V., Anikin, L., Petrovsky, V., and Karpov, G., A biogenic organ polymers in products of modern volcanism, *Ural. Geol. Zhurn.,* 2018b, no. 3, pp. 40–51.

Silaev, V.I., Karpov, G.A., Anikin, L.P., Vasiliev, E.A., Vergasova, L.P., and Smoleva, I.V., Mineral phase paragenesis in explosive ejecta discharged by recent eruptions in Kamchatka and the Kuril Islands. Part 1. Diamonds, carbonaceous phases, and condensed organoids, *J. Volcanol. Seismol.,* 2019a, vol. 13, no. 5, pp. 323–334.

Silaev, V.I., Karpov, G.A., Anikin, L.P., Vergasova, L.P., Filippov, V.N., and Tarasov, K.V., Mineral Phase Paragenesis in Explosive Ejecta Discharged by Recent Eruptions in Kamchatka and on the Kuril Islands. Part 2.

Accessory Minerals of the Tolbachik Type Diamonds, *J. Volcanol. Seismol.,* 2019b, vol. 13, no. 6, pp. 376–388.

Silaev, V.I., Proskurnin, V.F., Golubeva, I.I., et al., Penolites: A new type of endogenous rock, Belkovsky Island, Russia, *Vestnik Perm. Univers., Geologiya,* 2019, vol. 18, no. 2, pp. 125–147.

Svyatlovsky, A.E. and Kitaigorodsky, Yu.I., *Geodinamicheskaya vulkanologiya* (Geodynamic Volcanology), Moscow: Nedra, 1988.

Tarasov, L.S., Nazarov, M.A., Shevallevsky, I.D., et al., Rock petrography and the composition of regolith minerals from Mare Crisium, in *Lunnyi grunt iz Morya Krizisov* (Lunar Soil from Mare Crisium), Moscow: Nauka, 1980, pp. 78–95.

Taylor, S.R. and McLennan, S.M., *The Continental Crust: Its Composition and Evolution,* Blackwell Scientif. Publs., Oxford, 1985.

Tazieff, H., *Erebus: Volcan antarctique,* Arthaud, 1978.

Tonarini, S., D'Orazio, M., Armenti, P., et al., Geochemical features of Eastern Sicily lithosphere as probed by Hyblean xenoliths and lavas, *Eur. J. Mineral.,* 1996, vol. 8, pp. 1153–1173

Vai, G.B., Crustal evolution and basement elements in the Italian area: Palaeogeography and characterization, *Bull. Geofis. Teor. Appl.,* 1994, vol. 36, pp. 141–144.

Vai, G.B., Development of the palaeogeography of Pangaea from Late Carboniferous to Early Permian, *Palaeogeogr. Palaeoclim. Palaeoecol.,* 2003, vol. 196, pp. 125–155.

Voitkevich, G.V., Kokin, A.V., Miroshnikov, A.E., and Prokhorov, V.G., *Spravochnik po geokhimii* (A Handbook of Geochemistry), Moscow: Nedra, 1990.

Wood, D.A., The application of a Th-Hf-Ta diagram to problems of tectonomagmatic classification and to establishing the nature of crustal contamination of basaltic lavas of the British Tertiary Volcanic Province, *Earth Planet. Sci. Lett.,* 1980, vol. 50, pp. 11–30.

Translated by A. Petrosyan